International Symposium
On Turbulence and Shear Flow
Phenomena (TSFP-9)
June 30 - July 3, 2015 *Melbourne, Australia*

EXPERIMENTAL ANALYSIS OF TURBULENT FRICTION DRAG REDUCTION DUE TO SPANWISE TRANSVERSAL SURFACE WAVES

D. Roggenkamp*, W. Li, P. Meysonnat, M. Klaas, and W. Schröder
Institute of Aerodynamics
RWTH Aachen University
Wüllnerstraße 5a, Aachen, Germany
* Corresponding author: D.Roggenkamp@aia.rwth-aachen.de

ABSTRACT

The effectiveness of an active drag control method for turbulent boundary layers based on spanwise traveling transversal surface waves is investigated experimentally by micro-particle tracking velocimetry (μ-PTV) and particle-image velocimetry (PIV) above and downstream of the actuated surface. The experimental setup consists of a flat plate equipped with an insert that generates the spanwise traveling wave by electromagnetic actuators. The frequency and the wavelength are kept constant while the amplitude in inner coordinates is varied in the range of A^+=6 to 9. The experiments are performed at a Reynolds number $Re_\theta = 1200$ based on the momentum thickness directly downstream of the actuated surface. A detailed analysis of the phase-averaged flow field above the actuated surface based on the PIV results shows that the rms-distributions of the streamwise and wall-normal velocity fluctuations are increased in the outer part of the boundary layer. The probability function of u' and v' indicates that the ejections in the turbulent boundary layer are increased while the sweep events are decreased resulting in a lower friction drag. This result is confirmed by μ-PTV measurements downstream of the surface resulting in a drag reduction of up to 3.4 % dependent on the amplitude.

INTRODUCTION

The global warming and the lack of resources are intensified by a growing energy demand due to an increasing productivity and a greater urbanization accompanied by higher mobility. Therefore, especially in the transport sector it is essential to responsibly deal with energy resources. Regarding attached flows over slender bodies, i.e. airfoils, the friction drag is with approximately 50 % the main contributor to the total drag. To reduce the friction drag characterized by the wall-shear stress distribution one promising way is to control the near-wall flow structures. Besides, passive control methods like riblets many active approaches have been investigated. Most of these investigations concentrate on in-plane motion, such as spanwise oscillating walls. The effectiveness of this control mechanism has been verified especially for internal flows, i.e. turbulent channel or pipe flows by numerous numerical (e.g., Choi (2002), Touber and Leschziner (2012)) and experimental studies (e.g., Park et al. (2003), Ricco (2004)), resulting in a drag reduction ratio (*DR*) between 10 % and 45 %, where *DR* is defined as the relative wall-shear stress difference between the modified and the non-impacted flow. Other control methods of in-plane motion are for example rotating discs investigated by Ricco and Hahn (2013) or spanwise traveling waves without a transversal deflection analyzed by Du et al. 2002.

In contrast to the popular method of in-plane motion control there is the induction of a wall normal component to the near-wall flow by implementing a spanwise traveling transversal surface wave with wall normal deflection.

External flows, such as the turbulent flow over a flat plate subjected to the motion of transversal traveling surface waves were investigated by Klumpp et al. (2011), resulting in a *DR* of up to 9 %. The key feature of this drag reducing mechanism was found to be a damping of the wall-normal vorticity fluctuations and a resulting decrease of turbulence production. Koh et al. (2014) performed an LES to investigate the effect of a spanwise traveling wave dependent on the Reynolds number and the wave amplitude. The results show that the influence of the wave increases with increasing amplitude and decreasing Reynolds number.

Tamano and Itoh (2012) analyzed the effect of spanwise traveling waves with wall deformation experimentally using a flexible sheet. The cross hot-wire results showed a maximum *DR* of 13 % at a non-dimensional amplitude of $A^+ = 24$ and period of $T^+ = 115$. More recently, Roggenkamp et al. (2015) investigated experimentally the influence of a spanwise traveling surface wave on a turbulent boundary layer flow over an actuated aluminum surface. The results show that the velocity fluctuation in the outer boundary layer are increased while the streamwise momentum in the near-wall regime is lowered leading to a *DR* of up to 3.4% as a function of the amplitude. A comparison of numerical and experimental data performed by Meysonnat et al. (2015) substantiates these findings. In both studies the results of the experimental investigation are based on velocity measurements directly downstream of the surface.

The innovative character of this study is constituted by the challenge to measure the velocity field above the actuated surface synchronized with the wave motion. The former experimental investigations (Tamano and Itoh 2012, Roggenkamp et al. 2015, Meysonnat et al.) concentrated only on time- but not on phase-averaged velocity measurements. The synchronized PIV measurements in this study enable the investigation of the

Table 1. Flow parameters; the normalized parameters are defined in inner wall units by $T^+ = u_\tau^2/(f\nu)$, $\lambda^+ = \lambda\, u_\tau/\nu$, $A^+ = A\, u_\tau/\nu$, where the friction velocity uτ is determined for the non-actuated surface and ν represents the kinematic viscosity

Parameter	Dimensional	Non-dimensional
Velocity	U_∞ = 8 m/s	Re_θ = 1200
Frequency	f =81 Hz	T^+ = 110
Wave length	λ = 160 mm	λ^+ = 3862
Amplitude	A = 0.25- 0.375 mm	A^+ = 6-9

direct influence of the amplitude variation on the flow field above the wave trough and the wave crest down to a wall-normal distance in inner coordinates of y^+=13. To validate the PIV results they are compared with the numerical data of Meysonnat et al. (2015). Furthermore, the resulting drag reduction is determined by micro-particle tracking velocimetry (μ-PTV) directly downstream of the surface.

EXPERIMENTAL SETUP

In the following, the experimental setup is presented. A detailed description of the setup can be found in the study of Roggenkamp et al. (2015). The setup shown in Figure 1 consists of a flat plate mounted in the open 1.8 m×1.2 m test section of a low speed closed-loop wind tunnel with a tripping wire (d=0,5 mm) to generate a fully developed turbulent boundary layer. The actuated surface area is located in the center of the plate. To get close to engineering conditions the actuated surface consists of an aluminum sheet of 0.3 mm thickness.

The traveling sinusoidal wave is induced by an electromagnetic actuator system which is fixed underneath the aluminum sheet depicted in Figure 1. It has been developed by the Central Institute for Electronics (ZEL) of the Forschungszentrum Jülich. Details of the newly developed actuator system can be found in the study of Dück et al. (2015). The actuator system allows the generation of wave amplitudes to the aluminum surface up to A=0.5 mm with frequencies in the range 0 Hz<f<160 Hz and a minimum wave length of 60 mm.

To investigate the effect of the spanwise traveling wave on the flow field above the surface synchronized PIV measurements are performed. The synchronization of laser, camera, and actuator system enables the separate investigation of the flow field above the wave trough as well as above the wave crest. Furthermore, PIV and μ-PTV measurements are conducted 2 mm downstream of the actuated surface. Figure 1 shows the measurement setup with the laser light sheet positioned along the centerline of the PIV/μ-PTV setup and the corresponding camera arrangement. The different measurement positions are marked by MP1 and MP2. All measurements are conducted for the Reynolds number Re_θ = 1200 based on the freestream velocity and the momentum thickness immediately downstream of the actuated surface at a fixed wave length and frequency but at a changing amplitude. The dimensional flow quantities and the non-dimensional flow parameters in inner wall units, i.e., T^+, λ^+, and A^+, are summarized in Table 1.

MEASUREMENT TECHNIQUES AND EXPERIMENTAL UNCERTAINTIES

The PIV/μ-PTV arrangement is illustrated in Figure 1. At the first measurement position (MP1) above the actuated surface the velocity field is measured by standard 2C PIV with a measurement area of 30×30 mm². The light sheet is aligned in the streamwise direction. Downstream of the actuated surface (MP2), the flow field is measured on the one hand, by the standard 2C PIV described above and on the other hand, by μ-PTV to resolve the near-wall flow field. The wall-shear stress distribution is determined by the velocity gradient in the viscous sublayer. Since the viscous sublayer thickness is in the order of 0.2 mm (y^+=5) at the measurement plane a high resolution μ-PTV measurement system is applied. The Infinity™ K2® model long-distance microscope equipped with the Standard Objective is used to resolve a measurement area of 2×2 mm². Due to the low particle density in the near wall region, it is necessary to use particle tracking algorithms instead of standard PIV cross-correlation techniques.

The camera, the light sheet, and the actuator system are triggered by an external synchronizer such that the measurements are phase-averaged above the wave trough and the wave crest.

For both measurement methods the seeding particles, consisting of de-ethyl-hexal-sebacat (DEHS), possess the same mean diameter of 2-4 µm. For the PIV measurements global seeding is used whereas for the μ-PTV measurements a local seeding method is necessary to intensify the particle distribution in the near-wall region and to reduce absorption by the particles between the long-distance microscope and the measurement plane.

For each parameter configuration, 1362 image pairs are acquired by the PIV technique and 6810 for the µ-PTV measurements, which after post-processing are temporally averaged to obtain the final velocity data. To determine the flow field, the PIV data are evaluated using the commercial PIVview® software. The interrogation window size has 24 × 24 pixels with an overlap of 50 %. A camera calibration based on a polynomial model is applied to the images to reduce the distortion caused by the optical systems and the angle of view which is necessary to resolve the near-wall region in the wave trough.

The PTV data are analyzed using a Matlab® tracking routine. To average the data, the images are divided into intervals parallel to the wall of 10 µm ($0.24 < y^+ < 0.45$) height. The velocity vectors of each interval are averaged over all image pairs. Thus, the resulting mean values show the velocity profile in the near-wall region. The ratio between the particle spacing in one image Δx_p and the particle displacement between the images of an image pair Δx is 7.25. For synthetic particle images a ratio of 5 already results in almost 100 % valid links between particles.

The assumed minimum error of the PIV routine of 0.05 – 0.1 pixel leads to a relative measurement error of about 1 % outside the boundary layer at the freestream velocity of 8 m/s and to a relative error of about 2 %

inside the boundary layer close to the wall where the streamwise velocity is approximately 4 m/s.

The theoretical error of the mean velocity $\bar{u}$ on a 95 % confidence interval is $\Delta u = 1.96\sqrt{var(\bar{u})}$ with $var(\bar{u}) = \overline{u'^2}/N$. The maximum error based on $\bar{u}$ of the PIV data is 1.3 %. For the µ-PTV data, the maximum error is 1.2 % in the near-wall region $y^+ < 15$. In the region $y^+ > 15$, it is less than 0.8 %.

More details, concerning the measurement techniques and the experimental uncertainties, are given in the study of Roggenkamp et al. (2015).

RESULTS

In the following, the effect of the spanwise traveling transversal surface wave on the turbulent boundary layer is investigated. First, the PIV results above the actuated surface are analyzed to determine the influence of different wave amplitudes on the flow field with focus on the velocity fluctuations in the streamwise and wall-normal direction. Subsequently, the PIV and μ-PTV results downstream of the actuated surface are presented to discuss the impact of different wave amplitudes on the wall-shear stress distribution.

To determine the velocity distribution above the wave trough and the wave crest the PIV measurements are synchronized with the wave motion. The results of the mean streamwise velocity profile and the rms-distributions of the velocity fluctuations in the streamwise and wall-normal direction are compared with the numerical LES data of Meysonnat et al. (2015) for the non-actuated case and the configuration with maximum amplitude $A^+ = 9$. Both, the numerical and experimental data are analyzed at the measurement position MP1 at $x = 772$ mm (Figure 1). Note that in the following presentations of the results the wall distance is always given in relative coordinates, i.e., the zero position is moving together with the wall.

Figure 2 displays the comparison of the mean streamwise velocity profile above the wave trough (left) and the wave crest (right) at several amplitudes. Similar to the results of the measurements downstream of the actuated surface there is hardly any influence of the actuation on the streamwise velocity profile in the outer region of the boundary layer for both the wave trough and the wave crest. The comparison of the numerical and the experimental data show a convincing agreement.

Figure 3 depicts the distributions of the root-mean-square (rms) value of the streamwise velocity fluctuations scaled by the friction velocity of the non-actuated configuration at several amplitudes. Regarding the PIV data, at the wave trough (left) as well as at the wave crest (right) the velocity fluctuations in the streamwise direction are increased in the outer part of the boundary layer ($y^+ > 100$). At the wave trough this effect increases with increasing amplitude. The results at the wave crest show an opposite behavior. Thus, the distributions at the wave trough and the wave crest are shifted apart with increasing amplitude. Comparing the rms-distributions of the wall-normal velocity fluctuations of the PIV measurements illustrated in Figure 4, this influence of the actuation is even more evident.

This increase of the velocity fluctuations in the outer part of the boundary layer indicates that the turbulence content is shifted away from the wall to the outer part of the boundary layer. Thus, due to the induced momentum by the wall-normal motion the integral turbulence production occurs further off the wall, resulting in a decrease of the wall-shear stress. This effect depends on the direction of the induced motion and on the amplitude. Considering the differences in the rms-distributions of the velocity fluctuations in streamwise and wall-normal direction at the wave trough and the wave crest, the shift of the distributions off the wall amplitude dependent is more distinct at the wave trough. Thus, the downward motion induced by the moving wall reflected by the results at the wave trough is the dominant influencing factor. Again, the results show a convincing correspondence between the experimental and the numerical data. However, the influence of the wall motion on the rms-distributions of the velocity fluctuations is not clearly reflected by the LES data. Note that the amplitude in this study is rather low due to the technically relevant surface material aluminum. Thus, the influence of the surface motion on the flow field is very small such that the sensitivity of the numerical simulation is not strong enough to reveal the changes in the rms-distributions. Koh et al. (2014) also investigated numerically the influence of spanwise traveling waves on external turbulent boundary layer flow at a higher amplitude A^+=50. Their LES data confirm the findings of the current PIV results showing the same tendency of higher velocity fluctuation values in the outer part of the boundary layer due to the surface actuation.

Figure 5 shows the comparison of the joint probability density function (PDF) of u' and v' at $y^+ = 170$ of the non-actuated case and the case of maximum amplitude $A^+ = 9$ at the wave trough and the wave crest. The velocity fluctuations are non-dimensionalized by the rms-values of the non-actuated case. Usually, the events in second quadrant Q2 define ejections and the events in fourth quadrant Q4 determine sweeps causing local areas of high shear stress at the wall. The current results show that the most significant effect of the spanwise motion is that the PDF is shifted from Q4 to Q2. The effect is more distinct above the wave trough. Thus, on the one hand, the ejections are increased especially due to higher positive v' components on the other hand, the sweep events are decreased by the actuation, resulting in a reduced friction drag.

These findings are confirmed by the PIV and μ-PTV measurements 2 mm downstream of the actuated surface (MP2). The measurement position is depicted in Figure 1.

Figure 6 shows the mean streamwise velocity distribution at several amplitudes in comparison with the non-actuated configuration. The velocity distribution in the near-wall region was measured by μ-PTV whereas the velocity profile of the outer boundary layer was determined by PIV. Both data sets overlap in the region of $12 < y^+ < 22$. The good match of the data sets indicates a high quality of the results. At a first glance, there seems to be nearly no influence of the surface actuation on the velocity distribution. However, the near-wall flow field in the viscous sublayer illustrated in Figure 6 (right) in linear

Table 2. Drag ratio *DR* for the non-actuated case and the actuated configurations immediately downstream of the actuated surface

A^+	0	6	7	9
DR	0.0	2.0	2.7	3.4

scaling clearly shows lower velocity gradients for all actuated configurations in comparison to the non-actuated case. Using the wall-shear stress τ_w determined by

$$\tau_W = \mu \frac{\partial u}{\partial y}\Big|_{y=0} \approx \mu \frac{du}{dy}\Big|_{y=0} \quad (1)$$

the drag-reduction ratio *DR* is calculated by the skin-friction coefficient $c_f = \tau_W/(1/2\,\rho {u_\infty}^2)$

$$DR = \left(1 - \frac{c_{f,actuated}}{c_{f,non-actuated}}\right) \times 100\ \% \quad (2)$$

The results depicted in Table 2 evidence that the friction drag is reduced due to the spanwise traveling wave. The effect is enhanced by an increase of the wave amplitude.

CONCLUSIONS

The influence of a spanwise traveling transversal surface wave on a turbulent boundary layer has been investigated experimentally by μ-PTV and PIV above and downstream of the actuated surface. The Reynolds number based on the momentum thickness located directly downstream of the actuated surface was Re_θ = 1200. The wave motion was generated by a newly developed actuator system which enabled the actuation of a technical relevant aluminum surface at different amplitudes while the wave length and frequency have been kept constant. A detailed analysis of the velocity fluctuations in streamwise and wall-normal direction has been performed based on the PIV results above the actuated surface. The comparison with the numerical LES data of Meysonnat et al. (2015) shows a convincing agreement. The rms-distributions are affected by the spanwise traveling wave whereby the influence above the wave trough is clearer than above the wave crest. In both cases, the distributions are shifted dependent on the amplitude to higher values in the outer part of the boundary layer. This indicates a redistribution of the turbulence content off the wall leading to a lower momentum exchange in the viscous sublayer. Thus, the near-wall kinetic energy is decreased and the wall-shear stress is reduced. These findings are underlined by the joint PDF of *u*' and *v*'. The PDF is shifted from quadrant Q4 to Q2. This behavior is associated with an increase of ejections and a decrease of sweep events and thus a decreased wall-shear stress. The μ-PTV results downstream of the surface confirm the drag reducing effect. They show a clear impact of the surface actuation on the near-wall flow field resulting in a reduction of the friction drag up to DR = 3.4 % dependent on the amplitude.

ACKNOWLEDGEMENT

The support of this research by the Deutsche Forschungsgemeinschaft DFG in the frame of FOR 1779 is gratefully acknowledged.

REFERENCES

Choi, K.-S, 2002, "Near-wall structure of turbulent boundary layer with spanwise-wall oscillation", *Physics of Fluids*, Vol. 14, pp. 2530-2542.

Du, Y., Symeonidis, V., and Karniadakis, G., 2002, "Drag reduction in wall-bounded turbulence via a transverse travelling wave", *Journal of Fluid Mechanics*, Vol. 457, pp. 1-34.

Dück, M., Völkel, S., van Waasen, S., Schiek, M., and Abel, D., 2015, „Entwicklung einer echtzeitigen Aktuator-Ansteuerung mit Transienten-Glättung in LabVIEW Real-Time zur Strömungsregelung durch transversale Oberflächenwellen“, VDI Automation 2015.

Klumpp, S., Meinke, M., and Schröder, W., 2011, "Friction drag variation via spanwise transversal surface waves", *Flow, Turbulence and Combustion*, Vol. 87, pp. 33-53.

Koh, S., Meysonnat, P., Meinke, M., and Schröder, W., 2014, "Drag Reduction via Spanwise Transversal Surface Waves at High Reynolds Numbers", *submitted to Flow, Turbulence and Combustion.*

Koh, S., Meysonnat, P., Statnikov, V., Meinke, M., and Schröder, W., 2014, "Amplitude variation of spanwise transversal surface waves to lower turbulent wall-shear stress", *submitted to Computers & Fluids.*

Meysonnat, P., Roggenkamp, D., Li, W., Roidl, B., Schröder, W., 2015, "*Experimental and Numerical Investigation of Transversal Traveling Surface Waves for Drag Reduction"*, submitted to European Journal of Mechanics – Fluids.

Park, J., Hennoch, C., McCamley, M., and Breuer, K. S., 2003, "Lorentz Force Control of Turbulent Channel Flow", *33rd AIAA Fluid Dynamics Conference and Exhibit*, Orlando, Florida, AIAA Paper No. 2003-4157.

Ricco, P., 2004, "Modification of near-wall turbulence due to spanwise wall oscillations", *Journal of Turbulence*, Vol. 5, pp. 1-18.

Ricco, P., and Hahn, S., 2013, "Turbulent drag reduction through rotating discs", *Journal of Fluid Mechanics*, Vol. 722, pp. 267-290.

Roggenkamp, D., Jessen, W., Li, W., Klaas, M., and Schröder, W., 2015, "Experimental investigation of turbulent boundary layers over transversal moving surfaces", *submitted to CEAS Aeronautical Journal.*

Tamano, S., and Itoh, M., 2012, "Drag reduction in turbulent boundary layers by spanwise traveling waves with wall deformation", *Journal of Turbulence*, Vol. 13, pp. 1-26.

Touber P., and Leschziner, M., 2012, "Near-wall streak modification by spanwise oscillatory wall motion and drag-reduction mechanisms", *Journal of Fluid Mechanics*, Vol. 693, pp. 1-51.

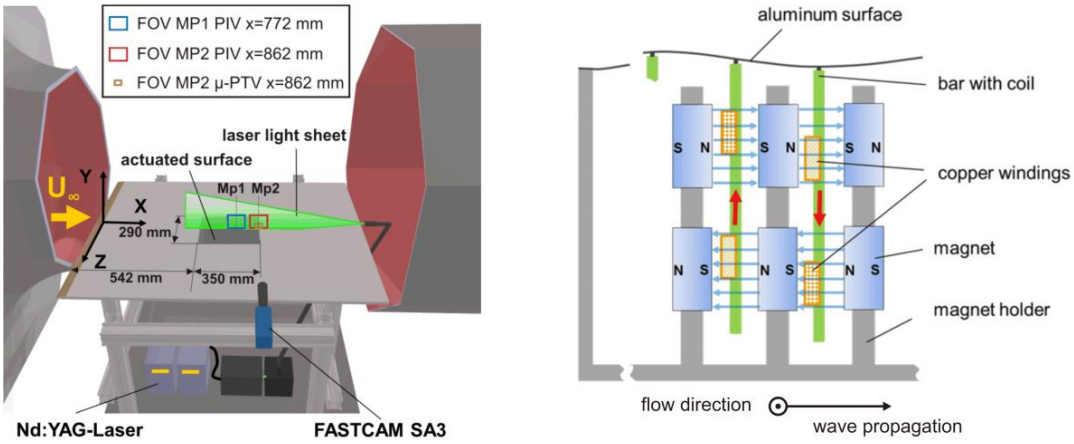

Figure 1. Sketch of the experimental setup showing the actuated surface, the PIV/μ-PTV arrangement with the corresponding measurement areas (left) and the electromagnetic actuator system (right)

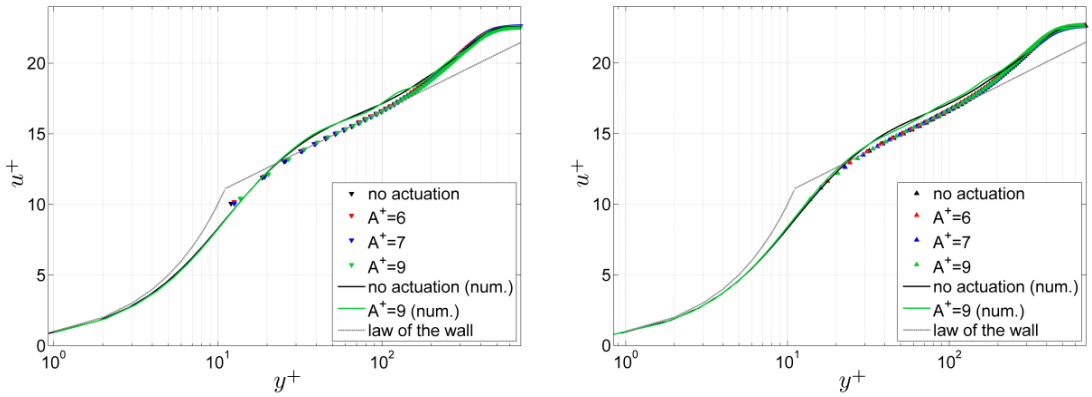

Figure 2. Comparison of the experimental (trough▼, crest▲) and numerical (—) mean streamwise velocity distributions above the actuated area at several amplitudes A^+ with the non-actuated case at the wave trough (left) and the wave crest (right); inner wall units are defined by the friction velocity u_τ of the non-actuated surface; the log law is defined by $\boldsymbol{u^+ = (1/0.4)\ln y^+ + 5.1}$

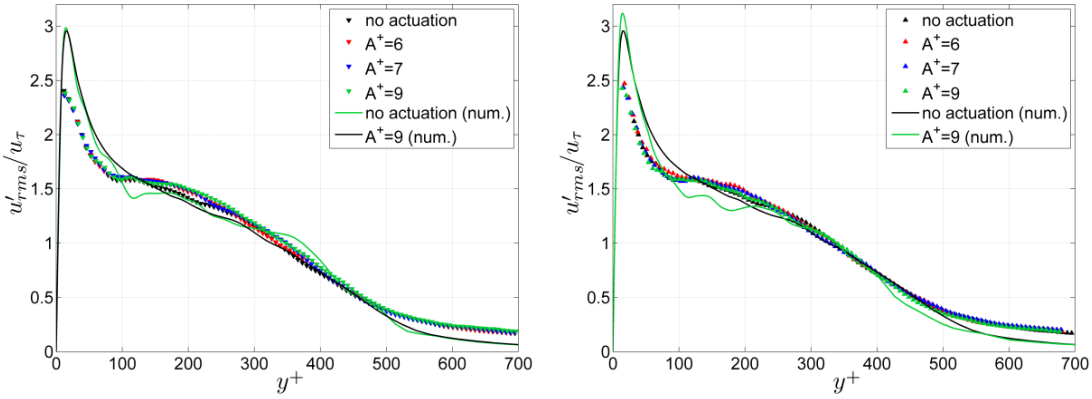

Figure 3. Comparison of the experimental (trough▼, crest▲) and numerical (—) root-mean square value of the streamwise velocity scaled by the friction velocity u_τ of the non-actuated surface above the actuated area at several amplitudes A^+ with the non-actuated case at the wave trough (left) and the wave crest (right); inner wall units are defined by the friction velocity u_τ of the non-actuated surface

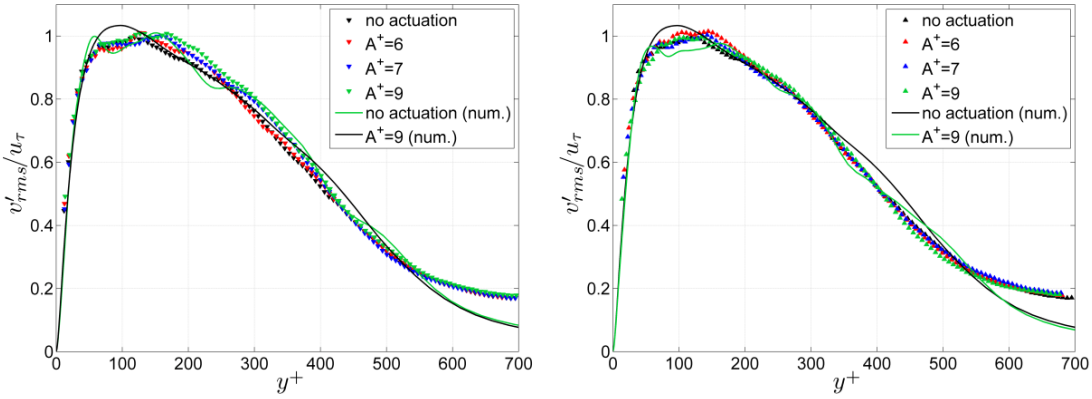

Figure 4. Comparison of the experimental (trough ▼, crest ▲) and numerical (—) root-mean square value of the wall-normal velocity scaled by the friction velocity u_τ of the non-actuated surface above the actuated area at several amplitudes A^+ with the non-actuated case at the wave trough (left) and the wave crest (right); inner wall units are defined by the friction velocity u_τ of the non-actuated surface

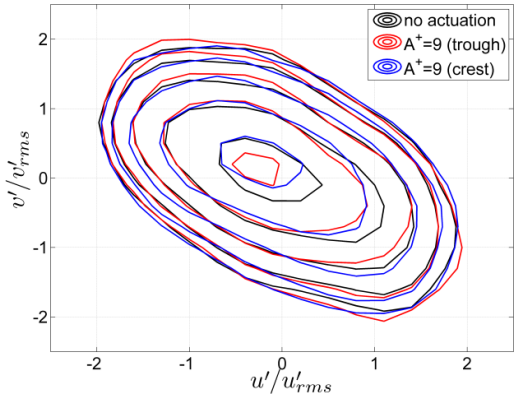

Figure 5. Comparison of the experimental joint PDF of u' and v' at y^+=170 above the actuated area at the amplitude A^+=9 with the non-actuated case

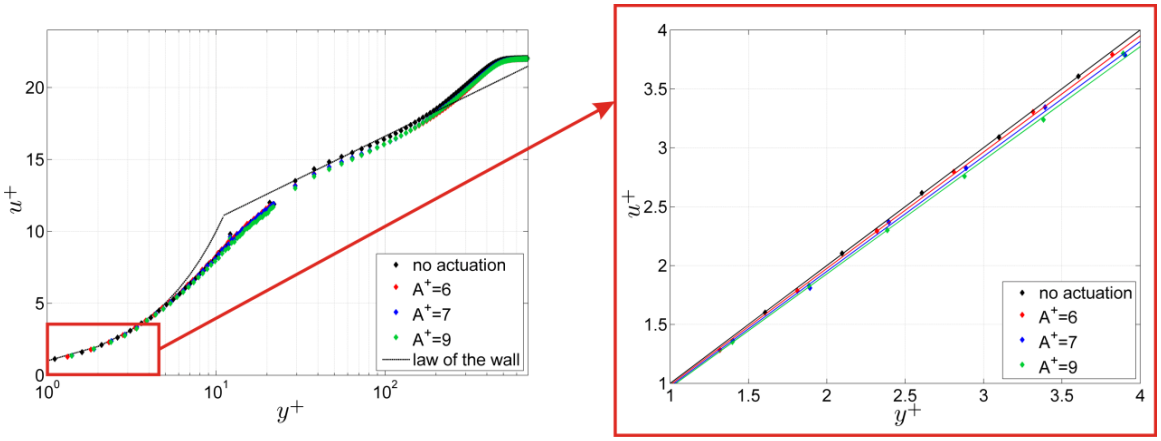

Figure 6. Comparison of the mean streamwise velocity distributions above the actuated area at several amplitudes A^+ with the non-actuated case; inner wall units are defined by the friction velocity u_τ of the non-actuated surface; the log law is defined by $\boldsymbol{u^+ = (1/0.4)\ln y^+ + 5.1}$; note that the enlarged illustration (right) has a linear scale